Cylindrical vector wave functions and applications in a source-free uniaxial chiral medium

Dajun Cheng and Yahia M. M. Antar
Department of Electrical and Computer Engineering, Royal Military College of Canada, Kingston, Ontario, Canada K7K 5L0
(Received 11 July 1997)

The uniaxial chiral medium, which is a modification of well-studied reciprocal chiral material, can be created by embedding microscopic metal helices in an isotropic host medium in such a way that the axes of all helices are oriented parallel to a fixed direction but distributed in random locations. Based on the concept of characteristic waves and the method of angular spectral expansion, cylindrical vector wave functions are rigorously developed to represent the electromagnetic fields in a source-free uniaxial chiral medium. Analysis reveals that the solutions of the source-free vector wave equation for uniaxial chiral medium, which are composed of two transverse waves and a longitudinal wave, can be represented in sum-integral forms of the cylindrical vector wave functions. The addition theorem of the vector wave functions for a uniaxial chiral medium can be directly obtained from its counterpart for the isotropic medium. To widen the application scope of the present cylindrical vector wave functions in a uniaxial chiral medium, a generalized mode-matching method is also proposed to study the two-dimensional electromagnetic scattering of a cylinder with an arbitrary cross section, and a conducting circular cylinder with an inhomogeneous coating thickness. To check the convergence of the present cylindrical vector wave functions for the multiple-body problem, electromagnetic scattering of two circular cylinders of uniaxial chiral media is also investigated. Excellent convergence properties of the cylindrical vector wave functions in these application examples are numerically verified, which establishes the reliability and applicability of the present cylindrical vector wave functions.
[S1063-651X(97)08312-8]

PACS number(s): 41.20.Jb, 03.40.Kf

I. INTRODUCTION

Vector wave functions, which were first proposed by Hansen to study electromagnetic radiation problems [1], are important concepts in electromagnetism. This concept, which was extensively developed by Stratton [2], Morse and Feshbach [3], and Tai [4] in studying electromagnetic boundary-value problems, seems to be gaining increasing interest and importance. Vector wave functions have found versatile applications, and presented great advantages compared with other methods (e.g., the three-dimensional moment method [5], the coupled-dipole method [6], and integral-equation technique [7]). However, the vector wave functions in any given complex media need to be developed, in order to provide methodological convenience in studying the electromagnetic properties of these materials. Recently, based on the concept of characteristic waves and the method of angular spectral expansion, electromagnetic field representations in unbounded and bounded source-free composite chiral-ferrite media were developed in terms of the cylindrical vector wave functions of isotropic media [8]. Most recently, Green dyadics in unbounded source-incorporated reciprocal uniaxial bianisotropic media [9] and uniaxial bianisotropic semiconductor material [10] have been formulated in terms of the cylindrical vector wave functions, using the concept of spectral eigenwaves and their completeness properties. Additionally, employing the Ohm-Rayleigh method, the dyadic Green's function in an unbounded gyroelectric chiral medium was expressed in the full eigenfunction expansion of the cylindrical vector wave functions [11]. Nevertheless, much effort is still needed, and to establish the reliability and applicability of the vector wave functions in studying the physical properties of the complex media, convergence properties of the series involved must be extensively examined.

There are basically five analytical and numerical methods, which are based on the eigenfunction solution of the wave equation, to investigate the electromagnetic phenomena, i.e., the mode-matching method [12], the perturbation approach [13], the T-matrix method [14], the point-matching method [15], and the multipole technique [16]. Despite the fact that the mode-matching method can provide rigorous criteria for other numerical methods, it is applicable only to simple boundary-value problems, which allow the Helmholtz equation to have a separation of variable-based solution. The perturbation method, which involves a Taylor expansion of the fields on the boundary, requires the smallness of the boundary perturbation, so that the higher order terms can be neglected. Although the T-matrix method has been widely employed to study electromagnetic boundary-value problems of isotropic media, this formulation, derived from Huygens's principle and the extinction theorem, requires that the Green dyadic in the exterior region must be expressible in terms of the eigenfunctions. Furthermore, due to the limited knowledge about Huygens's principle and the extinction theorem in complex material, it is often very difficult to obtain the T-matrix formulation. These constraints on the T-matrix method make it unsuitable to investigate the boundary-value problems of complex materials, where we cannot obtain the eigenfunction expansion of the Green dyadic. (For complex materials, the solution of the source-incorporated problems, which involves the Green dyadic, is much more difficult than the source-free one.) Although the point-matching method is not limited by the same constraint condition as T-matrix method, it is well-known that it is more time consuming for far-from-circular or -spherical geometry problems. The mul-

tipole technique, which requires a knowledge of the eigenfunction expansion of the field distribution of the unit source, is difficult to explore for investigating the physical phenomena of complex materials. Considering the applicability scope of the mode-matching method, perturbation approach, *T*-matrix formulation, point-matching method, and multipole technique, other computational approaches based on the vector wave functions, which should be superior to these already existing methods, still need to be studied so as to provide methodological convenience in investigating and exploring the physical phenomena involved in complex materials.

With recent advances in polymer synthesis techniques, increasing attention is being paid to the analysis of the interaction of electromagnetic waves with composite materials, in order to determine how to use these materials to provide better solutions to current engineering problems [17–19]. Recently, Lindell and co-workers [20–22] proposed a uniaxial chiral medium, and investigated the polarization properties of plane-wave reflection from a planar interface and propagation through a slab consisting of this material. It was predicted that such a medium could be more easily fabricated that the well-studied reciprocal chiral media [17,19]. Nevertheless, the nonplanar boundary-value problem of a uniaxial chiral medium still remains to be studied, so as to determine, interpret, and explore the physical properties of the curved structure of uniaxial chiral medium.

The uniaxial chiral medium, formed by immersing small metal helices in an isotropic host medium in such a way that the axes of all helices are oriented parallel to a fixed direction (the z axis) but distributed in random locations, is a subset of the wider class referred to as bianisotropic media. Excellent works in general bianisotropic media have been done by Post [23], Kong [12], and Chen [24], among others. In contradistinction to these general considerations, the present investigation is intended to develop the cylindrical vector wave functions to represent electromagnetic fields in a source-free uniaxial chiral medium, and to propose a generalized mode-matching method to study the two-dimensional electromagnetic boundary-value problems of uniaxial chiral medium. The present formulations of the cylindrical vector wave functions are considerably facilitated by using the concept of a characteristic wave and the method of angular spectrum expansion [8]. This extended method leads to compact and explicit expressions of the field representations in terms of the cylindrical vector wave functions. Furthermore, to make the efficient recursive algorithm developed by Chew [25] available to layered structures and multiscatterers consisting of uniaxial chiral media, an outline to derive the addition theorem of the vector wave functions for a uniaxial chiral medium is described. For applications of the present cylindrical vector wave functions, a generalized mode-matching method is proposed to study the two-dimensional electromagnetic scattering of a cylinder with an arbitrary cross section and a conducting circular cylinder with an inhomogeneous coating thickness. To check the convergence of the present cylindrical vector wave functions for a multiple-body problem, electromagnetic scattering by two circular cylinders of uniaxial chiral media is also investigated. Excellent convergence properties of the cylindrical vector wave functions in these application examples are numerically verified, which establishes the reliability and applicability of the present formulation.

This manuscript is organized as follows. In Sec. II, based on the concept of characteristic waves and the method of angular spectral expansion [8], the cylindrical vector wave functions in a source-free uniaxial chiral medium are developed to represent the electromagnetic field. It is found that the solutions of the source-free vector wave equation for a uniaxial chiral medium are composed of two transverse waves and a longitudinal wave. An addition theorem of the vector wave functions for a uniaxial chiral medium can be directly obtained from its counterpart for an isotropic medium. In Sec. III, to illustrate how to use the present cylindrical vector wave functions in a practical way, and examine the convergence properties of the infinite series involved, a generalized mode-matching method is proposed to study the electromagnetic scattering of a uniaxial chiral cylinder with an arbitrary cross section, and a conducting circular cylinder with an inhomogeneous coating thickness of a uniaxial chiral medium. To check the convergence of the present cylindrical vector wave functions for a multiple-body problem, electromagnetic scattering by two circular cylinders of uniaxial chiral media is also investigated. The formulations for these numerical calculations are briefly described in this context, and for the sake of consistency the details are arranged in the Appendixes. Extensive computations reveal that the infinite series involved in these application examples have excellent convergence properties, which establishes the reliability and applicability of the present cylindrical vector wave functions. Section IV concludes this manuscript with a remark on the present cylindrical vector wave functions and the generalized mode-matching method.

In the following analysis, a harmonic $\exp(i\omega t)$ time dependence is assumed and suppressed. In the notations we adopt, a double underline is used to represent dyadics, and boldface is used for vectors.

II. CYLINDRICAL VECTOR WAVE FUNCTIONS

From a phenomenological point of view, a homogeneous uniaxial chiral medium can be characterized by the set of constitutive relations [20–22]

$$\mathbf{D}=\underline{\underline{\varepsilon}}\cdot\mathbf{E}-\underline{\underline{\xi}}\cdot\mathbf{H}, \tag{1a}$$

$$\mathbf{B}=\underline{\underline{\mu}}\cdot\mathbf{H}+\underline{\underline{\xi}}\cdot\mathbf{E}, \tag{1b}$$

where $\underline{\underline{\varepsilon}}=\varepsilon_t(\mathbf{e}_x\mathbf{e}_x+\mathbf{e}_y\mathbf{e}_y)+\varepsilon_z\mathbf{e}_z\mathbf{e}_z$, and $\underline{\underline{\mu}}=\mu_t(\mathbf{e}_x\mathbf{e}_x+\mathbf{e}_y\mathbf{e}_y)+\mu_z\mathbf{e}_z\mathbf{e}_z$ are the permittivity and permeability dyadics, respectively. $\underline{\underline{\xi}}=\xi\mathbf{e}_z\mathbf{e}_z$ is the magnetoelectric pseudodyadic, and ξ is specifically related to the chirality parameter ξ_c by the equation $\xi=i\xi_c(\mu_0\varepsilon_0)^{1/2}$, where μ_0 and ε_0 are the permittivity and permeability of free space, respectively. Here $\mathbf{e}_j$ denotes the unit vector in the j direction. For a lossless uniaxial chiral medium, the constitutive parameters ε_t, ε_z, μ_t, μ_z, and ξ_c are all real. Obviously, the constitutive parameters of uniaxial chiral medium satisfy the reciprocal conditions [12], therefore such a medium is reciprocal. It should be noted that the present formulations do not require any constraint conditions on the constitutive parameters, and hence they can be applied for both lossy and lossless uniaxial chiral medium.

Different from [8] which starts with the **H**-field vector wave equation, the present starting point will be the **E**-field one. To this end, substituting the constitutive relations (1a) and (1b) into the source-free Maxwell equations, an **E**-field vector wave equation in this composite medium is obtained:

$$\nabla\times\underline{\mu}^{-1}\cdot\nabla\times\mathbf{E}+i\omega(\nabla\times\underline{\mu}^{-1}\cdot\underline{\xi}\cdot\mathbf{E}-\underline{\xi}\cdot\underline{\mu}^{-1}\cdot\nabla\times\mathbf{E}) -\omega^2(\underline{\varepsilon}-\underline{\xi}\cdot\underline{\mu}^{-1}\cdot\underline{\xi})\cdot\mathbf{E}=\mathbf{0}. \tag{2}$$

The characteristic waves of Eq. (2) can be examined in the Fourier spectral domain by introducing the transformation

$$\mathbf{E}(\mathbf{r})=\int_{-\infty}^{\infty}\int_{-\infty}^{\infty}\int_{-\infty}^{\infty}\mathbf{E}(\mathbf{r})e^{-i\mathbf{k}\cdot\mathbf{r}}dk_x dk_y dk_z, \tag{3}$$

where $\mathbf{k}=k_x\mathbf{e}_x+k_y\mathbf{e}_y+k_z\mathbf{e}_z$. Substituting Eq. (3) into Eq. (2), algebraic manipulation leads to

$$\int_{-\infty}^{\infty}\int_{-\infty}^{\infty}\int_{-\infty}^{\infty}\underline{\mathbf{W}}\cdot\mathbf{E}(\mathbf{k})dk_x dk_y dk_z=0, \tag{4}$$

where

$$\underline{\mathbf{W}}=\begin{bmatrix} k_z^2+\mu' k_y^2-a & -\mu' k_x k_y & -k_x k_z+bk_y \\ -\mu' k_x k_y & k_z^2+\mu' k_x^2-a & -k_y k_z-bk_x \\ -k_x k_z-bk_y & -k_y k_z+bk_x & k_x^2+k_y^2-a' \end{bmatrix},$$

with

$$a=\omega^2\varepsilon_t\mu_t,$$

$$b=\omega\mu'\xi,$$

$$a'=\omega^2(\varepsilon_z\mu_t+\mu'\xi^2),$$

and $\mu'=\mu_t/\mu_z$. For nontrivial solutions of Eq. (4), the determinant of matrix $\underline{\mathbf{W}}$ operating on $\mathbf{E}(\mathbf{k})$ must be equal to zero. Straightforward algebraic manipulation results in the characteristic equation

$$\mu' a k_\rho^4+(k_z^2-a)(a+\mu' a'-b^2)k_\rho^2+(k_z^2-a)^2 a'=0, \tag{5}$$

where $k_\rho^2=k_x^2+k_y^2$.

In the following analysis, the roots of Eq. (5) are designated as $k_\rho=k_{\rho q}$ ($q=1$, 2, 3, and 4), which are functions of k_z. The eigenvectors of Eq. (4), expressed in a circular cylindrical coordinate system, can be easily obtained from Eq. (4) in association with the coordinate transformation

$$\mathbf{E}_q(k_z,\phi_k)=[A_q(k_z)\cos(\phi-\phi_k)+B_q(k_z)\sin(\phi-\phi_k)]\mathbf{e}_\rho +[-A_q(k_z)\sin(\phi-\phi_k)+B_q(k_z)\cos(\phi-\phi_k)] \times\mathbf{e}_\phi+\mathbf{e}_z, \tag{6}$$

where

$$A_q(k_z)=\frac{k_{\rho q}k_z}{k_z^2-a}, \tag{7a}$$

$$B_q(k_z)=\frac{bk_{\rho q}}{(\mu' k_{\rho q}^2+k_z^2-a)}, \tag{7b}$$

and $\phi_k=\tan^{-1}(k_y/k_x)$, and $\phi=\tan^{-1}(y/x)$.

Returning to Eq. (3), and noting $k_{\rho 3}=-k_{\rho 1}$ and $k_{\rho 4}=-k_{\rho 2}$, we can represent the electric field in terms of the above-introduced eigenvectors

$$\mathbf{E}(\mathbf{r})=\sum_{q=1}^{2}\int_{\phi_k=0}^{2\pi}d\phi_k\int_{-\infty}^{\infty}dk_z e^{-i[k_z z+k_{\rho q}\rho\cos(\phi-\phi_k)]} \times\mathbf{E}_q(k_z,\phi_k)E_{qz}(k_z,\phi), \tag{8}$$

where $\rho=(x^2+y^2)^{1/2}$, and $E_{qz}(k_z,\phi_k)$ is the amplitude of the spectral longitudinal component of the electric field. The symmetric roots $k_{\rho 3}$ and $k_{\rho 4}$ are not included in the summation of Eq. (8), since they are automatically taken into account as the spectral azimuthal angle ϕ_k spans from 0 to 2π.

Substituting Eq. (6) into Eq. (8), the solution $\mathbf{E}(\mathbf{r})$ of the source-free vector wave equation (2) for an infinite uniaxial chiral medium can be expressed in terms of the scalar cylindrical wave functions. However, in order to have a tractable solution for boundary-value problems involving cylindrical structures of uniaxial chiral media, it is required to transform the expansion of Eq. (8) into a form resembling the vector wave solution for an isotropic medium. To this end, applying the angular spectral expansion to $E_{qz}(k_z,\phi_k)$, under the hypothesis that $E_{qz}(k_z,\phi_k)$ is continuous and separable with respect to its variables, yields

$$E_{qz}(k_z,\phi_k)=\sum_{n=-\infty}^{\infty}e_{qn}(k_z)e^{-in\phi_k},$$

and we have

$$\mathbf{E}(\mathbf{r})=\sum_{q=1}^{2}\int_{-\infty}^{\infty}dk_z\sum_{n=-\infty}^{\infty}e_{qn}(k_z)\mathbf{E}_{qn}(k_z), \tag{9}$$

where

$$\mathbf{E}_{qn}(k_z)=\int_{\phi_k=0}^{2\pi}d\phi_k e^{-i[k_z z+k_{\rho q}\rho\cos(\phi-\phi_k)+n\phi_k]}\mathbf{E}_q(k_z,\phi_k). \tag{10}$$

It is worth noting that in the process of obtaining Eq. (9) from Eq. (8), the integration order for k_z and ϕ_k has been exchanged, because the integrand is continuous in the range $[0,2\pi]\times(-\infty,+\infty)$.

Substituting into Eq. (10) the well-known identity

$$e^{-ik_{\rho q}\rho\cos(\phi-\phi_k)}=\sum_{m=-\infty}^{\infty}(-i)^m J_m(k_{\rho q}\rho)e^{-im(\phi-\phi_k)}, \tag{11}$$

and its derivatives with respect to ρ and ϕ, after lengthy mathematical manipulation by grouping properly the terms involving in the integration for the ϕ_k variable and introducing the cylindrical vector wave functions, we end up with (see Appendix A for detail)

$$\mathbf{E}(\mathbf{r})=\pi\sum_{q=1}^{2}\int_{-\infty}^{\infty}dk_z\sum_{n=-\infty}^{\infty}(-i)^n e_{qn}(k_z)[A_q^e(k_z)\times\mathbf{M}_n^{(1)}(k_z,k_{\rho q})+B_q^e(k_z)\mathbf{N}_n^{(1)}(k_z,k_{\rho q})+C_q^e(k_z)\times\mathbf{L}_n^{(1)}(k_z,k_{\rho q})], \tag{12}$$

where the cylindrical vector wave functions are defined as

$$\mathbf{M}_n^{(j)}(k_z,k_{\rho q})=\nabla\times[\Psi_n^{(j)}(k_z,k_{\rho q})\mathbf{e}_z], \tag{13a}$$

$$\mathbf{N}_n^{(j)}(k_z,k_{\rho q})=\frac{1}{k_q}\nabla\times\mathbf{M}_n^{(j)}(k_z,k_{\rho q}), \tag{13b}$$

$$\mathbf{L}_n^{(j)}(k_z,k_{\rho q})=\nabla[\Psi_n^{(j)}(k_z,k_{\rho q})], \tag{13c}$$

with $k_q=(k_{\rho q}^2+k_z^2)^{1/2}$. Here the generating function is defined as $\Psi_n^{(j)}(k_z,k_{\rho q})=Z_n^{(j)}(k_{\rho q}\rho)\exp[-i(k_z z+n\phi)]$, and

$$Z_n^{(j)}(k_{\rho q}\rho)=\begin{cases}J_n(k_{\rho q}\rho), & j=1\\ Y_n(k_{\rho q}\rho), & j=2\\ H_n^{(1)}(k_{\rho q}\rho), & j=3\\ H_n^{(2)}(k_{\rho q}\rho), & j=4.\end{cases} \tag{13d}$$

Since Bessel, Neumann, and Hankel functions of the same order satisfy the identical differential equation, the first kind of vector wave functions in Eq. (12) can be generalized to three other kinds corresponding to Neumann and Hankel functions.

In Eq. (12), the weighted coefficients of the vector wave functions are found to be

$$A_q^e(k_z)=-\frac{2ib}{k_z^2+\mu' k_\rho^2 q^{-a}}, \tag{14a}$$

$$B_q^e(k_z)=-\frac{2a}{k_q(k_z^2-a)}, \tag{14b}$$

$$C_q^e(k_z)=\frac{2ik_z(k_q^2-a)}{k_q^2(k_z^2-a)}. \tag{14c}$$

The representation for the magnetic field can be easily obtained from the Maxwell curl equation in association with Eqs. (1a) and (1b)

$$\mathbf{H}=\underline{\underline{T}}^T\cdot\underline{\underline{\mu}}^{-1}\cdot\underline{\underline{T}}\left[\frac{i}{\omega}(\nabla\times\mathbf{E})-\underline{\underline{T}}^T\cdot\underline{\underline{\xi}}\cdot\underline{\underline{T}}\cdot\mathbf{E}\right], \tag{15}$$

where

$$\underline{\underline{T}}=\begin{bmatrix}\cos\phi & -\sin\phi & 0\\ \sin\phi & \cos\phi & 0\\ 0 & 0 & 1\end{bmatrix}$$

is the coordinate transformation matrix [25], and the superscript T denotes the transpose of a matrix. Substituting Eq. (12) into Eq. (15), after algebraic manipulation we obtain

$$\mathbf{H}(\mathbf{r})=\pi\sum_{q=1}^{2}\int_{-\infty}^{\infty}dk_z\sum_{n=-\infty}^{\infty}(-i)^n e_{qn}(k_z)[A_q^h(k_z)\times\mathbf{M}_n^{(1)}(k_z,k_{\rho q})+B_q^h(k_z)\mathbf{N}_n^{(1)}(k_z,k_{\rho q})+C_q^h(k_z)\times\mathbf{L}_{qn}^{(11)}(k_z,k_{\rho q})], \tag{16}$$

where the weighted coefficients of the vector wave functions are determined as

$$A_q^h(k_z)=\frac{ik_q}{\omega\mu_c}B_q^e(k_z), \tag{17a}$$

$$B_q^h(k_z)=\frac{1}{\mu_t k_q}\left\{\frac{i}{\omega}(k_z^2+\mu' k_{\rho q}^2)A_q^e(k_z)-\mu'\xi\left[\frac{k_{\rho q}^2}{k_q}B_q^e(k_z)-ik_z C_q^e(k_z)\right]\right\}, \tag{17b}$$

$$C_q^h(k_z)=\frac{k_z A_q^e(k_z)}{\omega\mu_t}+\frac{ik_z B_q^h(k_z)}{k_q}. \tag{17c}$$

The resulting Eqs. (12) and (16) indicate that solutions of the source-free Maxwell equations in a uniaxial chiral medium, which can be represented in terms of the cylindrical vector wave functions, are superpositions of two transverse waves (TE for **M** and TM for **N**), and a longitudinal wave.

The other set of field representations can be straightforwardly obtained by proceeding with the **H**-field vector wave equation following the above-described procedure. Alternatively, they can be derived via the duality principle [12]. An addition theorem of the cylindrical vector wave functions for a uniaxial chiral medium can be directly obtained by substituting the counterpart for an isotropic medium [25] in Eqs. (12) and (16).

III. APPLICATIONS AND CONVERGENCE PROPERTIES OF THE CYLINDRICAL VECTOR WAVE FUNCTIONS

To illustrate how to use the present cylindrical vector wave functions in a practical way, and to examine the convergence properties of the infinite series involved, a generalized mode-matching method is proposed to study the electromagnetic scattering of a cylinder with an arbitrary cross section, and a conducting circular cylinder with an inhomogeneous coating thickness. To check the convergence of the present cylindrical vector wave functions for a multiple-body problem, electromagnetic scattering by two circular cylinders of uniaxial chiral media is also investigated.

A. An infinitely long cylinder with arbitrary cross section

In this subsection, we will try to develop a generalized mode-matching method to study the electromagnetic scattering of a cylinder with an arbitrary cross section. For this purpose, we first choose the coordinate system so that the incident wave is along the $+x$ axis. The cylinder is bounded by the surface $\rho=f(\phi)$, where $f'(\phi)$ is a single value and continuous function of ϕ.

Since an arbitrary polarized electromagnetic wave in free space can be decomposed into TM_z- and TE_z-polarized

waves which are independent and reciprocal with each other, we will only consider the TM_z incident case without losing any generality. The incident TM_z wave of unit amplitude is expanded in terms of the circular cylindrical vector wave functions

$$\mathbf{E}^{\mathrm{inc}}(\mathbf{r})=\mathbf{e}_z e^{-ik_0 x}=\int_{-\infty}^{\infty} dk_z \sum_{n=-\infty}^{\infty}(-i)^n \delta(k_z) \times \mathbf{N}_n^{(1)}(k_z,k_\rho)/k_0, \tag{18a}$$

$$\mathbf{H}^{\mathrm{inc}}(\mathbf{r})=-i\mathbf{e}_y e^{-ik_0 x}/\eta_0=\int_{-\infty}^{\infty} dk_z \sum_{n=-\infty}^{\infty}(-i)^{n-1} \delta(k_z) \times \mathbf{M}_n^{(1)}(k_z,k_\rho)/(k_0\eta_0), \tag{18b}$$

where $k_\rho=(k_0^2-k_z^2)^{1/2}$, and $\delta(\,)$ is the Dirac delta function. Here, $k_0=\omega(\mu_0\varepsilon_0)^{1/2}$ and $\eta_0=(\mu_0/\varepsilon_0)^{1/2}$ represents the wave number and incident wave impedance of the free space, respectively. The scattered electromagnetic waves may have TM_z and TE_z components, and should be expanded as

$$\mathbf{E}^{\mathrm{sca}}(\mathbf{r})=\int_{-\infty}^{\infty} dk_z \sum_{n=-\infty}^{\infty}(-i)^n[a_n\mathbf{M}_n^{(4)}(k_z,k_\rho)+b_n \times \mathbf{N}_n^{(4)}(k_z,k_\rho)], \tag{19a}$$

$$\mathbf{H}^{\mathrm{sca}}(\mathbf{r})=\int_{-\infty}^{\infty} k_z \sum_{n=-\infty}^{\infty}(-i)^{n-1}/\eta_0[a_n\mathbf{N}_n^{(4)}(k_z,k_\rho)+b_n \times \mathbf{M}_n^{(4)}(k_z,k_\rho)]. \tag{19b}$$

In expressions (18) and (19), the functions $\mathbf{M}_n^{(j)}(k_z,k_\rho)$ and $\mathbf{N}_n^{(j)}(k_z,k_\rho)$ ($j=1$ and 4) are the cylindrical vector wave functions as defined in Sec. II.

The electromagnetic fields excited inside the scatterer, $\mathbf{E}^{\mathrm{int}}(\mathbf{r})$ and $\mathbf{H}^{\mathrm{int}}(\mathbf{r})$, can be represented in terms of the cylindrical vector wave functions in the way we presented in Sec. II.

The boundary conditions to ensure the continuity of the electric and magnetic fields at the outer surface of the scatterer $\rho=f(\phi)$ are

$$E_\rho^{\mathrm{int}}\sin\theta+E_\phi^{\mathrm{int}}\cos\theta=(E_\rho^{\mathrm{inc}}+E_\rho^{\mathrm{sca}})\sin\theta+(E_\phi^{\mathrm{inc}}+E_\phi^{\mathrm{sca}})\cos\theta, \tag{20a}$$

$$E_z^{\mathrm{int}}=E_z^{\mathrm{inc}}+E_z^{\mathrm{sca}}, \tag{20b}$$

$$H_\rho^{\mathrm{int}}\sin\theta+H_\phi^{\mathrm{int}}\cos\theta=(H_\rho^{\mathrm{inc}}+H_\rho^{\mathrm{sca}})\sin\theta+(H_\phi^{\mathrm{inc}}+H_\phi^{\mathrm{sca}})\cos\theta, \tag{20c}$$

$$H_z^{\mathrm{int}}=H_z^{\mathrm{inc}}+H_z^{\mathrm{sca}}, \tag{20d}$$

where all the field components are evaluated at $\rho=f(\phi)$, and

$$\theta=\tan^{-1}\left(\frac{f'(\phi)}{f(\phi)}\right),$$

To solve Eqs. (20a)–(20d) numerically, the infinite series involved must be truncated. In what follows, the infinite summation is so truncated that the series is taken to be summed up from $-N$ to N. These truncated equations can easily be analytically solved for the expansion coefficients of the scattered fields. For the sake of consistency, details of formulations of the solution procedure are organized in Appendix B. After carefully examining the final numerical results, excellent convergent properties of these truncated series are established, which make the truncating process reasonable.

The bistatic echo width, which represents the density of the power scattered by the cylindrical object, is defined as

$$A_\sigma(\phi)=\lim_{\rho-\infty} 2\pi\rho\,\frac{\mathrm{Re}\{\mathbf{E}^{\mathrm{sca}}(\mathbf{r})\times[\mathbf{H}^{\mathrm{sca}}(\mathbf{r})]^*\}\cdot\mathbf{e}_\rho}{\mathrm{Re}\{\mathbf{E}^{\mathrm{inc}}(\mathbf{r})\times[\mathbf{H}^{\mathrm{inc}}(\mathbf{r})]^*\}\cdot\mathbf{e}_\rho}, \tag{21}$$

where the asterisk indicates complex conjugate, and Re{ } denotes the real part of the complex function.

Recalling the asymptotic expression of the Hankel function in the far region,

$$H_n^{(2)}(k_0\rho)=\left(\frac{2}{\pi k_0\rho}\right)^{1/2} e^{-i[k_0\rho-(2n+1)\pi/4]}, \quad \rho\to\infty, \tag{22}$$

we can rewrite expression (21) in a more explicit form,

$$A_\sigma(\phi)=4k_0\left[\left|\sum_{n=-\infty}^{\infty} a_n e^{-in\phi}\right|^2+\left|\sum_{n=-\infty}^{\infty} b_n e^{-in\phi}\right|^2\right], \tag{23}$$

To validate this generalized mode-matching process, numerical results of the present method for the scattering by a circular cylinder ($\rho=a$) and a deviated circular cylinder ($\rho=b\cos\phi+\sqrt{b^2\cos^2\phi+a^2-b^2}$, $b<a$) have been computed and compared with that of a circular cylinder calculated by the conventional mode-matching method, respectively. Excellent agreement between the results is obtained. For completeness and comparison purposes, formulations of the conventional mode-matching method for scattering by a circular cylinder are presented in Appendix C.

Prior to the actual computation for the scattering by a uniaxial chiral cylinder with a noncircular cross section, the convergence of the results involved must be examined. Table I presents the numerical results of the convergence test for a uniaxial chiral cylinder with an elliptical cross section. It is seen that by properly choosing the truncated number N of the series involved, reliable results can be obtained for all scattering angles. The convergence check indicates that the present cylindrical vector wave functions in conjunction with the generalized mode-matching method can be reliably applied to study the two-dimensional electromagnetic phenomena of a single uniaxial chiral object. To provide criteria for other numerical methods, Fig. 1 illustrates the bistatic echo width of an elliptical cylinder of a uniaxial chiral medium.

B. A conducting circular cylinder with an inhomogeneous coating thickness

In this subsection, we will try to use the generalized mode-matching method to study the electromagnetic scatter-

TABLE I. Convergence test of an elliptical cylinder of uniaxial chiral medium (TM_z). The constitutive parameters of the scatterer are taken to be $\varepsilon_t=2.5\varepsilon_0$, $\varepsilon_z=2.1\varepsilon_0$, $\mu_t=1.8\mu_0$, $\mu_z=1.2\mu_0$, and $\xi_c=-0.5$, and geometry parameters of the scatterer are taken to be semimajor axis$=1.6\lambda_0$, and semiminor axis$=1.3\lambda_0$. The major axial of the scatterer takes an angle of $3\pi/7$ with respect to the x axis. Square brackets indicate powers of 10.

A_σ/λ_0 (dB)	$\phi=0°$	$\phi=45°$	$\phi=90°$	$\phi=135°$	$\phi=180°$
$N=9$	0.16136[+02]	0.79976[+01]	−0.21696[+01]	−0.24474[+01]	0.18237[+01]
$N=10$	0.16522[+02]	0.87868[+01]	−0.20618[+01]	−0.48577[+01]	0.72725[+01]
$N=11$	0.16785[+02]	0.96647[+01]	−0.96852[+00]	−0.29797[+01]	0.83456[+01]
$N=12$	0.16981[+02]	0.84121[+01]	−0.23009[+01]	−0.25108[+01]	0.96109[+01]
$N=13$	0.17002[+02]	0.84512[+01]	−0.24026[+01]	−0.20637[+01]	0.96900[+01]
$N=14$	0.17012[+02]	0.84891[+01]	−0.24118[+01]	−0.19976[+01]	0.97280[+01]
$N=15$	0.17014[+02]	0.84748[+01]	−0.23930[+01]	−0.20095[+01]	0.97389[+01]
$N=16$	0.17014[+02]	0.84752[+01]	−0.23936[+01]	−0.20097[+01]	0.97393[+01]
$N=17$	0.17014[+02]	0.84753[+01]	−0.23954[+01]	−0.20132[+01]	0.97398[+01]
$N=20$	0.17014[+02]	0.84753[+01]	−0.23954[+01]	−0.20132[+01]	0.97398[+01]

ing of a conducting circular cylinder with an arbitrary coating thickness of a uniaxial chiral medium. For this purpose, we first fix the coordinate system so that the incident wave is along the $+x$ axis, the conducting core is bounded by $\rho=a$, and the outer surface is bounded by the surface $\rho=f(\phi)$, where $f'(\phi)$ is a single value and a continuous function of ϕ.

Once again, the TM_z incident wave with unit amplitude is considered. The incident and scattered waves are expanded in terms of the cylindrical vector wave functions, as Eqs. (18) and (19). According to the cylindrical vector wave functions in uniaxial chiral material developed in Sec. II, the fields in the coating region can be represented as

$$\mathbf{E}^{\text{int}}=\sum_{q=1}^{2}\sum_{n=-\infty}^{\infty}(-i)^n\{e_{qn}^{(1)}[A_q^e\mathbf{M}_n^{(1)}(k_{\rho q})+B_q^e\mathbf{N}_n^{(1)}(k_{\rho q})+C_q^e\mathbf{L}_n^{(1)}(k_{\rho q})]+e_{qn}^{(4)}[A_q^e\mathbf{M}_n^{(4)}(k_{\rho q})+B_q^e\mathbf{N}_n^{(4)}(k_{\rho q})+C_q^e\mathbf{L}_n^{(4)}(k_{\rho q})]\}, \tag{24a}$$

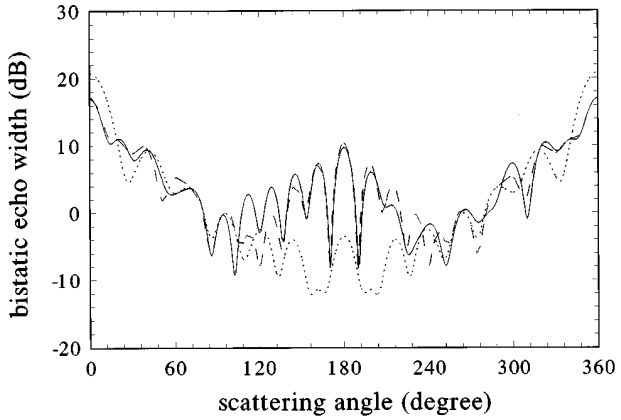

FIG. 1. Scattering pattern of an elliptical uniaxial chiral cylinder due to a normally incident TM_z-polarized plane wave. The constitutive parameters are $\varepsilon_t=2.5\varepsilon_0$, $\varepsilon_z=2.1\varepsilon_0$, $\mu_t=1.8\mu_0$, $\mu_z=1.2\mu_0$, and $\xi=-0.5i(\varepsilon_0\mu_0)^{1/2}$. The geometry parameters of the scatters are the semimajor axis $1.6\lambda_0$ and the semiminor axis $1.3\lambda_0$. The dotted line corresponds to the case where the major axis of the scatterer is along the x axis, the dashed line is for the major axis along the y axis, and the solid line is for a major axis having an angle of $3\pi/7$ with respect to the x axis.

$$\mathbf{H}^{\text{int}}=\sum_{q=1}^{2}\sum_{n=-\infty}^{\infty}(-i)^n\{e_{qn}^{(1)}[A_q^h\mathbf{M}_n^{(1)}(k_{\rho q})+B_q^h\mathbf{N}_n^{(1)}(k_{\rho q})+C_q^h\mathbf{L}_n^{(1)}(k_{\rho q})]+e_{qn}^{(4)}[A_q^h\mathbf{M}_n^{(4)}(k_{\rho q})+B_q^h\mathbf{N}_n^{(4)}(k_{\rho q})+C_q^h\mathbf{L}_n^{(4)}(k_{\rho q})]\}, \tag{24b}$$

where $e_{qn}^{(1)}$ and $e_{qn}^{(4)}$ ($q=1$ and 2) are expansion coefficients. Here $k_z=0$ for the cylindrical vector wave functions, and their weighted coefficients have been suppressed for the sake of writing simplicity.

The boundary conditions at the boundary $\rho=a$ are

$$E_z^{\text{int}}|_{\rho=a}=0, \tag{25a}$$

$$E_\phi^{\text{int}}|_{\rho=a}=0, \tag{25b}$$

and the boundary conditions at the outer surface of the scatterer $\rho=f(\phi)$ are

$$E_\rho^{\text{int}}\sin\theta+E_\phi^{\text{int}}\cos\theta=(E_\rho^{\text{inc}}+E_\rho^{\text{sca}})\sin\theta+(E_\phi^{\text{inc}}+E_\phi^{\text{sca}})\cos\theta, \tag{26a}$$

$$E_z^{\text{int}}=E_z^{\text{inc}}+E_2^{\text{sca}}, \tag{26b}$$

$$H_\rho^{\text{int}}\sin\theta+H_\phi^{\text{int}}\cos\theta=(H_\rho^{\text{inc}}+H_\rho^{\text{sca}})\sin\theta+(H_\phi^{\text{inc}}+H_\phi^{\text{sca}})\cos\theta \tag{26c}$$

$$H_z^{\text{int}}=H_z^{\text{inc}}+H_z^{\text{sca}}, \tag{26d}$$

where all the field components are evaluated at $\rho=f(\phi)$, and

$$\theta=\tan^{-1}\left(\frac{f'(\phi)}{f(\phi)}\right)$$

To solve Eqs. (25) and (26) numerically, the infinite series involved must be truncated. These truncated equations can be easily solved for the expansion coefficients of the scat-

TABLE II. Convergence test of a conducting circular cylinder with a coating of elliptical cross section (TM_z). The constitutive parameters of the scatterer are taken as $\varepsilon_t=2.5\varepsilon_0$, $\varepsilon_z=2.1\varepsilon_0$, $\mu_t=1.8\mu_0$, $\mu_z=1.2\mu_0$, and $\xi_c=0.5$. The elliptical-shaped coating has a semimajor axis of $1.3\lambda_0$ and semiminor axis of $1.1\lambda_0$, and the radius of the conducting cone is $0.8\lambda_0$. The major axial of the cross section of the coating takes an angle of $2\pi/7$ with respect to the x axis.

A_σ/λ_0 (dB)	$\phi=0°$	$\phi=45°$	$\phi=90°$	$\phi=135°$	$\phi=180°$
$N=9$	0.17262[+02]	0.35584[+01]	0.34753[+01]	0.79088[+01]	0.70301[+01]
$N=10$	0.17304[+02]	0.33819[+01]	0.37202[+01]	0.79704[+01]	0.71569[+01]
$N=11$	0.17311[+02]	0.34114[+01]	0.36576[+01]	0.80054[+01]	0.71605[+01]
$N=12$	0.17305[+02]	0.33271[+01]	0.36610[+01]	0.79730[+01]	0.71804[+01]
$N=13$	0.17304[+02]	0.33270[+01]	0.36639[+01]	0.79731[+01]	0.71780[+01]
$N=14$	0.17304[+02]	0.33271[+01]	0.36592[+01]	0.79706[+01]	0.71784[+01]
$N=15$	0.17304[+02]	0.33271[+01]	0.36592[+01]	0.79705[+01]	0.71753[+01]
$N=16$	0.17304[+02]	0.33329[+01]	0.36593[+01]	0.79705[+01]	0.71753[+01]
$N=17$	0.17304[+02]	0.33329[+01]	0.36593[+01]	0.79704[+01]	0.71753[+01]
$N=20$	0.17304[+02]	0.33329[+01]	0.36593[+01]	0.79704[+01]	0.71753[+01]

tered fields. For the sake of consistency, details of the formulations of the solution procedure are organized in Appendix D.

To validate this generalized mode-matching process, numerical results of the present method for the solution of a conducting circular cylinder with a coaxial coating are computed and compared with those calculated by the conventional mode-matching method. Excellent agreement between the results is obtained.

Similar to Sec. III A, a convergence test of the results involved should be carefully examined for the scattering of a conducting circular cylinder with an inhomogeneous coating thickness of a uniaxial chiral medium. Table II presents numerical results of the convergence test for a conducting circular cylinder with a uniaxial chiral coating of an elliptical cross section. It is seen that for a proper truncated number N, reliable results can be obtained for all scattering angles. The convergence check indicates that the present cylindrical vector wave functions, in association with the generalized mode-matching method, can be reliably utilized to investigate the two-dimensional boundary-value problem of multilayered uniaxial chiral objects. To provide criteria for other numerical method, Fig. 2 illustrates the bistatic echo width of a conducting circular cylinder with a uniaxial chiral coating of an elliptical cross section.

C. Two circular cylinders

To illustrate the applicability of the present cylindrical vector wave functions for multiple scattering problems, we now use the addition theorem to study the electromagnetic scattering of two circular cylinders consisting of uniaxial chiral media. The geometrical configuration of the cross section and symbols used here are illustrated in Fig. 3, where the constitutive relations for cylinder j $(j=1,2)$ are

$$\mathbf{D}=\underline{\varepsilon}_j\cdot\mathbf{E}-\underline{\xi}_j\cdot\mathbf{H}, \tag{27a}$$

$$\mathbf{B}=\underline{\mu}_j\cdot\mathbf{H}+\underline{\xi}_j\cdot\mathbf{E}, \tag{27b}$$

The normally incident plane wave of unit amplitude with an incident angle φ^{inc} with respect to the $+x$ axis can be expanded in terms of the cylindrical vector wave functions:

$$\mathbf{E}^{\text{inc}}(\mathbf{r})=\sum_{n=-\infty}^{\infty}(-i)^n[a_n^{\text{inc}}\mathbf{M}_n^{(1)}(k_0,\mathbf{r})+b_n^{\text{inc}}\mathbf{N}_n^{(1)}(k_0,\mathbf{r})], \tag{28a}$$

$$\mathbf{H}^{\text{inc}}(\mathbf{r})=\sum_{n=-\infty}^{\infty}(-i)^{n-1}/\eta_0[a_n^{\text{inc}}\mathbf{N}_n^{(1)}(k_0,\mathbf{r})+b_n^{\text{inc}}\times\mathbf{M}_n^{(1)}(k_0,\mathbf{r})], \tag{28b}$$

where $k_z=0$ in the vector wave functions has been suppressed, and the coordinate system in which the vector wave functions are used has been indicated by the position vector in the vector wave functions. For the TM_z-polarized incident

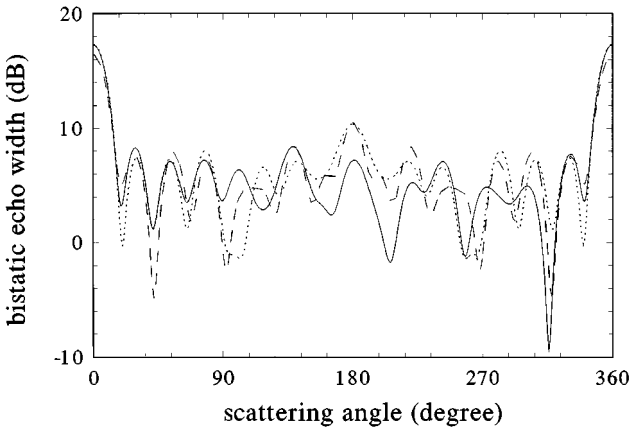

FIG. 2. Scattering pattern of a conducting circular cylinder with a coating of an elliptical cross section, due to a normally incident TM_z-polarized plane wave. The constitutive parameters of $\varepsilon_t=2.5\varepsilon_0$, $\varepsilon_z=2.1\varepsilon_0$, $\mu_t=1.8\mu_0$, $\mu_z=1.2\mu_0$, and $\xi=-0.5i(\varepsilon_0\mu_0)^{1/2}$. The elliptical-shaped coating has a semimajor axis of $1.3\lambda_0$ and semiminor axis of $1.1\lambda_0$, and the radius of the conducting cone is $0.8\lambda_0$. The dotted line corresponds to the case where the major axis of the coating is along the x axis, the dashed line is for the major axis along the y axis, and the solid line is for the major axis having an angle of $2\pi/7$ with respect to the x axis.

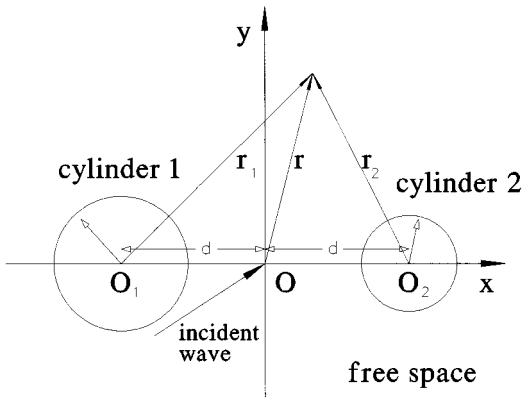

FIG. 3. Geometry configuration of the structure of two circular cylinders.

plane wave, $a_n^{\text{inc}}=0$ and $b_n^{\text{inc}}=e^{in\varphi^{\text{inc}}}/k_0$. For the TE_z-polarized incident plane wave, $a_n^{\text{inc}}=e^{in\varphi^{\text{inc}}}/k_0$ and $b_n^{\text{inc}}=0$.

The electromagnetic fields inside the scatterers can be separately expanded in terms of the cylindrical vector wave functions in local coordinate systems:

$$\mathbf{E}_j^{\text{int}}(\mathbf{r}_j)=\sum_{q=1}^{2}\sum_{n=-\infty}^{\infty}(-i)^n\{e_{qn}^{(j)}[A_q^{e(j)}\mathbf{M}_n^{(1)}(k_{\rho q}^{(j)},\mathbf{r}_j)+B_q^{e(j)}\mathbf{N}_n^{(1)}(k_{\rho q}^{(j)},\mathbf{r}_j)+C_q^{e(j)}\mathbf{L}_n^{(1)}(k_{\rho q}^{(j)},\mathbf{r}_j)], \tag{29a}$$

$$\mathbf{H}_j^{\text{int}}(\mathbf{r}_j)=\sum_{q=1}^{2}\sum_{n=-\infty}^{\infty}(-i)^n\{e_{qn}^{(j)}[A_q^{h(j)}\mathbf{M}_n^{(1)}(k_{\rho q}^{(j)},\mathbf{r}_j)+B_q^{h(j)}\mathbf{N}_n^{(1)}(k_{\rho q}^{(j)},\mathbf{r}_j)+C_q^{h(j)}\mathbf{L}_n^{(1)}(k_{\rho q}^{(j)},\mathbf{r}_j)] \tag{29b}$$

for $j=1$ and 2. Here $k_z=0$ in the weighted coefficients of the vector wave functions has been suppressed.

The scattered fields are the superpositions of those scattered from each cylinder,

$$\mathbf{E}^{\text{sca}}=\sum_{j=1}^{2}\mathbf{E}_j^{\text{sca}},\quad \mathbf{H}^{\text{sca}}=\sum_{j=1}^{2}\mathbf{H}_j^{\text{sca}}, \tag{30}$$

where $\mathbf{E}_j^{\text{sca}}$ and $\mathbf{H}_j^{\text{sca}}$ can be represented in the O_j coordinate system as

$$\mathbf{E}_j^{\text{sca}}(\mathbf{r}_j)=\sum_{n=-\infty}^{\infty}(-i)^n[a_n^{(j)}\mathbf{M}_n^{(4)}(k_0,\mathbf{r}_j)+b_n^{(j)}\mathbf{N}_n^{(4)}(k_0,\mathbf{r}_j)], \tag{31a}$$

$$\mathbf{H}_j^{\text{sca}}(\mathbf{r}_j)=\sum_{n=-\infty}^{\infty}(-i)^{n-1}/\eta_0[a_n^{(j)}\mathbf{N}_n^{(4)}(k_0,\mathbf{r}_j)+b_n^{(j)}\times\mathbf{M}_n^{(4)}(k_0,\mathbf{r}_j)], \tag{31b}$$

Based on the addition theorem for the Bessel and Hankel functions [25], the transformation of the cylindrical vector wave functions from the O_q coordinate to the O_p coordinate are obtained:

$$\mathbf{Q}_n^{(1)}(k,\mathbf{r}_q)=\sum_{m=-\infty}^{\infty}\mathbf{Q}_m^{(1)}(k,\mathbf{r}_p)J_{m-n}(kd_{pq})e^{i(m-n)\varphi_{pq}}, \tag{32a}$$

$$\mathbf{Q}_n^{(4)}(k,\mathbf{r}_q)=\sum_{m=-\infty}^{\infty}\mathbf{Q}_m^{(1)}(k,\mathbf{r}_p)H_{m-n}^{(2)}(kd_{pq})e^{i(m-n)\varphi_{pq}}, \tag{32b}$$

where $\mathbf{Q}=\mathbf{M}$ or $\mathbf{N}$, and (d_{pq},φ_{pq}) is the position of O_q in the O_p coordinate system.

Using the addition theorem of the cylindrical vector wave functions, and applying the boundary conditions at each surface of the scatterer to ensure the tangential components of electric and magnetic fields are continuous, a set of coupled linear equations involving the scattering coefficients are obtained. For the sake of consistency, details of the formulations of the solution procedure are organized in Appendix E.

The bistatic echo width of the scattering structure can be obtained by using the asymptotic expansion of the Hankel function, Eq. (22), and $\rho_{1,2}\approx\rho\pm d\cos\varphi$ for $\rho\to\infty$, which result in

$$A_\sigma=4k_0\left|\sum_{n=-\infty}^{\infty}e^{-in\varphi}(e^{-ik_0d\cos\varphi}b_n^{(1)}+e^{ik_0d\cos\varphi}b_n^{(2)})\right|^2+4k_0\left|\sum_{n=-\infty}^{\infty}e^{-in\varphi}(e^{-ik_0d\cos\varphi}a_n^{(1)}+e^{ik_0d\cos\varphi}a_n^{(2)})\right|^2. \tag{33}$$

For a TM_z-polarized incident plane wave, the first term in the right-hand side of Eq. (33) represents the copolarized echo width, and the second the cross-polarized one. For a TE_z-polarized incident plane wave, the first and second terms in Eq. (33) stand for the cross-polarized and copolarized echo widths, respectively.

Again, it is important to examine the convergence properties of the final results for the series involved in the scattering by two circular cylinders of uniaxial chiral media. Table III presents numerical results for the convergence test of this scattering structure. It is seen that for proper truncated number N, reliable results can be obtained for all scattering angles. The convergence check indicates that the present cylindrical vector wave functions can be reliably applied to study the two-dimensional multiple-body problem of uniaxial chiral media. To provide criteria for future references, Figs. 4 and 5 illustrates the bistatic echo width of two circular cylinders of uniaxial chiral media for TM_z and TE_z polarized incident wave, respectively (see also Table IV).

IV. CONCLUDING REMARKS

In the present investigation, cylindrical vector wave functions are developed to represent the electromagnetic field in a source-free uniaxial chiral medium. The formulation is greatly facilitated by using the concept of characteristic

TABLE III. Convergence test of two circular cylinders due to a TM_z polarized incident plane wave. The constitutive parameters of the media are taken to be $\mu_t^{(1)}=1.4\mu_0$, $\mu_z^{(1)}=1.2\mu_0$, $\varepsilon_t^{(1)}=2.5\varepsilon_0$, $\varepsilon_z^{(1)}=2.3\varepsilon_0$, and $\xi_c^{(1)}=-0.3$, and $\mu_t^{(2)}=1.3\mu_0$, $\mu_z^{(2)}=1.1\mu_0$, $\varepsilon_t^{(2)}=2.3\varepsilon_0$, $\varepsilon_z^{(2)}=2.2\varepsilon_0$, and $\xi_c^{(2)}=-0.5$. The geometry parameters of the scatterer are taken to be $a_1=0.4\lambda_0$, $a_2=0.7\lambda_0$, and $d=1.5\lambda_0$. The incident angle is $2\pi/9$.

A_σ/λ_0 (dB)	$\phi=0°$	$\phi=45°$	$\phi=90°$	$\phi=135°$	$\phi=180°$
$N=3$	0.59801[+01]	0.16374[+02]	0.22021[+01]	−0.26449[+00]	−0.37412[+01]
$N=4$	0.61982[+01]	0.17101[+02]	−0.21969[+00]	0.10312[+00]	0.77866[+00]
$N=5$	0.68301[+01]	0.17475[+02]	−0.14073[+00]	−0.43131[+01]	−0.35832[+01]
$N=6$	0.67600[+01]	0.17331[+02]	−0.33208[+00]	−0.11678[+01]	−0.57911[+01]
$N=7$	0.67632[+01]	0.17322[+02]	−0.34480[+00]	−0.12621[+01]	−0.57445[+01]
$N=8$	0.67629[+01]	0.17322[+02]	−0.34512[+00]	−0.12668[+01]	−0.57480[+01]
$N=9$	0.67629[+01]	0.17322[+02]	−0.34509[+00]	−0.12663[+01]	−0.57479[+01]
$N=10$	0.67629[+01]	0.17322[+02]	−0.34508[+00]	−0.12663[+01]	−0.57479[+01]

waves and the method of angular spectral expansion. The formulation developed here generalizes the canonical solutions of vector wave functions for isotropic media, and recovers the case of uniaxial media ($\xi=0$). For applications of cylindrical vector wave functions, a generalized mode-matching method is proposed to study the two-dimensional electromagnetic scattering of a uniaxial chiral cylinder with an arbitrary cross section and a conducting circular cylinder with an inhomogeneous coating thickness of a uniaxial chiral medium. To check the convergence of the present cylindrical vector wave functions for nontrivial problems (such as multiple-body problems), electromagnetic scattering by two circular cylinders of uniaxial chiral media is also investigated. Excellent convergence properties of the cylindrical vector wave functions in these application examples are numerically verified, which establishes the reliability and applicability of the present theory.

Here it is worthwhile to point out the differences between the present formulations and those of previous works [8–11]. (1) Noting the available results on the theory of cylindrical vector wave functions in an unbounded source-incorporated composite medium [9–11], the starting points of these formulations (i.e., the concept of spectral eigenwaves and their completeness properties, and the Ohm-Rayleigh method) would fail to work out to the present case, which treats the finite-region source-free medium. (2) Although the basis of the present formulations (i.e., the concept of a characteristic wave and the method of angular spectrum expansion) is the same as that of Ref. [8], they treat fundamentally different materials (i.e., the constitutive relations of the materials are different) and the starting points are different (the present formulation starts with the **E**-field vector wave equation, while Ref. [8] began with the **H**-field one). The present formulations can be considered as an alternative application example of the method of angular spectrum expansion. (3) In Ref. [8], only the simplest application example (i.e., the scat-

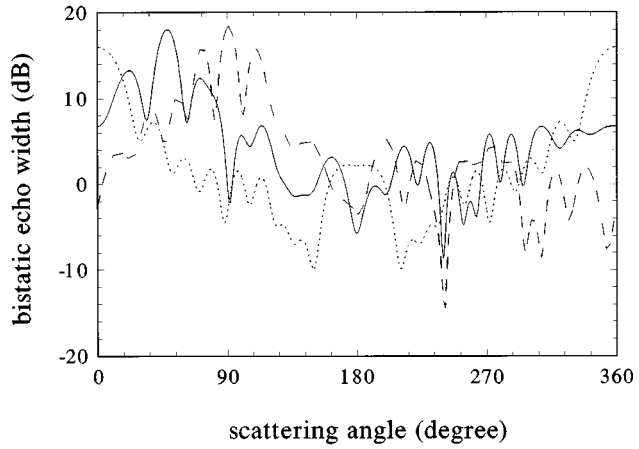

FIG. 4. Scattering pattern of two circular cylinders, due to a normally incident TM_z-polarized plane wave. The constitutive parameters of the cylinders are taken to be $\mu_t^{(1)}=1.4\mu_0$, $\mu_z^{(1)}=1.2\mu_0$, $\varepsilon_t^{(1)}=2.5\varepsilon_0$, $\varepsilon_z^{(1)}=2.3\varepsilon_0$, and $\xi_c^{(1)}=-0.3$, and $\mu_t^{(2)}=1.3\mu_0$, $\mu_z^{(2)}=1.1\mu_0$, $\varepsilon_t^{(2)}=2.3\varepsilon_0$, $\varepsilon_z^{(2)}=2.2\varepsilon_0$, and $\xi_c^{(2)}=-0.5$. The geometry parameters of the scatterer are $a_1=0.4\lambda_0$, $a_2=0.7\lambda_0$, and $d=1.5\lambda_0$. The dotted line corresponds to the case of $\varphi^{\rm inc}=0$, the dashed line to $\varphi^{\rm inc}=\pi/2$, and the solid line to $\varphi^{\rm inc}=2\pi/9$.

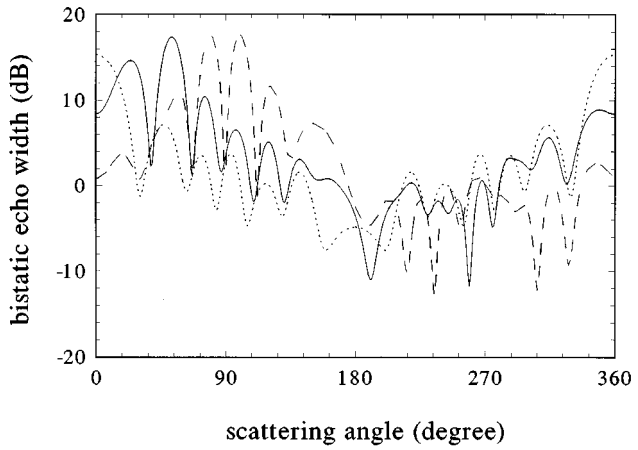

FIG. 5. Scattering pattern of two circular cylinders, due to a normally incident TE_z-polarized plane wave. The constitutive parameters of the coating are taken to be $\mu_t^{(1)}=1.4\mu_0$, $\mu_z^{(1)}=1.2\mu_0$, $\varepsilon_t^{(1)}=2.5\varepsilon_0$, $\varepsilon_z^{(1)}=2.3\varepsilon_0$, and $\xi_c^{(1)}=-0.3$, and $\mu_t^{(2)}=1.3\mu_0$, $\mu_z^{(2)}=1.1\mu_0$, $\varepsilon_t^{(2)}=2.3\varepsilon_0$, $\varepsilon_z^{(2)}=2.2\varepsilon_0$, and $\xi_c^{(2)}=-0.5$. The geometry parameters of the scatterer are $a_1=0.5\lambda_0$, $a_2=0.6\lambda_0$, and $d=1.3\lambda_0$. The dotted line corresponds to the case of $\varphi^{\rm inc}=0$, the dashed line to $\varphi^{\rm inc}=\pi/2$, and the solid line to $\varphi^{\rm inc}=2\pi/9$.

TABLE IV. Convergence test of two circular cylinders due to a TE_z-polarized incident plane wave. The constitutive parameters of the coating are taken to be $\mu_t^{(1)}=1.4\mu_0$, $\mu_z^{(1)}=1.2\mu_0$, $\varepsilon_t^{(1)}=2.5\varepsilon_0$, $\varepsilon_z^{(1)}=2.3\varepsilon_0$, and $\xi_c^{(1)}=-0.3$, and $\mu_t^{(2)}=1.3\mu_0$, $\mu_z^{(2)}=1.1\mu_0$, $\varepsilon_t^{(2)}=2.3\varepsilon_0$, $\varepsilon_z^{(2)}=2.2\varepsilon_0$, and $\xi_c^{(2)}=-0.5$. The geometry parameters of the scatterer are taken to be $a_1=0.5\lambda_0$, $a_2=0.6\lambda_0$, and $d=1.3\lambda_0$. The incident angle is $2\pi/9$.

A_σ/λ_0 (dB)	$\phi=0°$	$\phi=45°$	$\phi=90°$	$\phi=135°$	$\phi=180°$
$N=3$	0.50854[+01]	0.13746[+02]	−0.10151[+01]	−0.23631[+01]	0.76576[+00]
$N=4$	0.76736[+01]	0.14066[+02]	0.49795[+01]	0.37525[+00]	−0.51318[+01]
$N=5$	0.83736[+01]	0.13728[+02]	0.35951[+01]	0.68597[+00]	−0.33950[+01]
$N=6$	0.84118[+01]	0.13697[+02]	0.36374[+01]	0.86800[+00]	−0.35224[+01]
$N=7$	0.84116[+01]	0.13694[+02]	0.36486[+01]	0.85633[+00]	−0.35213[+01]
$N=8$	0.84114[+01]	0.13694[+02]	0.36490[+01]	0.85583[+00]	−0.35207[+01]
$N=9$	0.84114[+01]	0.13694[+02]	0.36490[+01]	0.85588[+00]	−0.35207[+01]
$N=10$	0.84114[+01]	0.13694[+02]	0.36490[+01]	0.85588[+00]	−0.35207[+01]

tering of an infinitely long circular cylinder) was considered, while the present work reports more complicated applications (i.e., electromagnetic scattering by a cylinder of an arbitrary cross section, a conducting circular cylinder with an inhomogeneous coating thickness, and two circular cylinders). Moreover, a convergence check of the results in these complicated application examples are extensively examined, which establishes the reliability and applicability of the present cylindrical vector wave functions for more complex structures. (4) To make use of the present cylindrical vector wave functions in the complicated applications, a generalized mode-matching method is proposed, and numerical implementation is extensively carried out in the present work.

It should be pointed out that the generalized mode-matching method presented here, although not requiring the eigenfunction expansion of the Green dyadic, is applicable only to small aspect-ratio scatterers like the conventional T-matrix method. For large aspect-ratio scatterers, the challenge of convergence and time consumption must be taken into account. However, this method is obviously superior to the conventional mode-matching method [12,25], which can only be applicable to a circular cylindrical structure, the perturbation method [13] which is only suitable to a near-circular cylindrical structure, and the T-matrix method [14] and multipole technique [16], both of which require a knowledge of a source-incorporated solution, and may be regarded as the modified form of the point-matching method [15], since they can be utilized under the same conditions and have the same challenges for a complex structure. Using the addition theorem of the cylindrical vector wave functions and the formulations for a single scatterer, a homogenization theory for the uniaxial chiral composite media may be established, where a pair-distributed function can result from experiment, theoretical investigation, or numerical results.

It is of interest to note that the cylindrical vector wave functions can be expanded as discrete sums of the spherical vector wave functions [26]; therefore the present cylindrical vector wave functions could be extended to solve problems of spherical structures. Although excellent convergence and efficiency of the present cylindrical vector wave functions in tackling the two-dimensional physical phenomena have been demonstrated by extensive numerical computation, one should carefully examine the convergence and efficiency of the theory in actual computation when using the spherical vector wave functions for three-dimensional electromagnetic phenomena. Nevertheless, it is believed that the present cylindrical vector wave functions and the generalized mode-matching method would be helpful in analyzing and exploiting the physical phenomena associated with the boundary-value problems of layered structures, as well as multiscatterers consisting of uniaxial chiral media.

APPENDIX A: DETAIL OF THE FIELD REPRESENTATIONS

Substituting expressions (6) and (11) in Eq. (9), we have the electric field expanded in terms of the eigenvectors in a circular cylindrical coordinate system

$$\begin{aligned}\mathbf{E}(\mathbf{r})=\sum_{q=1}^{2}\int_{-\infty}^{\infty}dk_z\sum_{n=-\infty}^{\infty}e_{qn}(k_z)\int_{\phi_k=0}^{2\pi}d\phi_k\\ \times e^{-i[k_z z+k_{\rho q}\rho\cos(\phi-\phi_k)]}\{[A_q(k_z)\cos(\phi-\phi_k)\\ +B_q(k_z)\sin(\phi-\phi_k)]\mathbf{e}_\rho+[-A_q(k_z)\sin(\phi-\phi_k)\\ +B_q(k_z)\cos(\phi-\phi_k)]\mathbf{e}_\phi+\mathbf{e}_z\}\end{aligned}\tag{A1}$$

Taking the derivatives of Eq. (11) with respect to ρ and ϕ, respectively, we have

$$\begin{aligned}&\cos(\phi-\phi_k)e^{-ik_{\rho q}\rho\cos(\phi-\phi_k)}\\ &\quad=\sum_{m=-\infty}^{\infty}(-i)^{m-1}\frac{\partial J_m(k_{\rho q}\rho)}{k_{\rho q}\partial\rho}e^{-im(\phi-\phi_k)}\end{aligned}\tag{A2}$$

and

$$\begin{aligned}&\sin(\phi-\phi_k)e^{-ik_{\rho q}\rho\cos(\phi-\phi_k)}\\ &\quad=-\sum_{m=-\infty}^{\infty}(-i)^{m}\frac{mJ_m(k_{\rho q}\rho)}{k_{\rho q}\rho}e^{-im(\phi-\phi_k)}.\end{aligned}\tag{A3}$$

Inserting Eqs. (A2), (A3) and (11) into Eq. (A1), we obtain

$$\mathbf{E}(\mathbf{r})=\sum_{q=1}^{2}\int_{-\infty}^{\infty}dk_z\sum_{n=-\infty}^{\infty}e_{qn}(k_z)[P_n(k_z)\mathbf{e}_\rho+Q_n(k_z)\mathbf{e}_\phi+R_n(k_z)\mathbf{e}_z], \tag{A4}$$

where

$$\begin{aligned}P_n(k_z)&=\int_{\phi_k=0}^{2\pi}d\phi_k\sum_{m=-\infty}^{\infty}\left[(-i)^{m-1}\frac{\partial J_m(k_{\rho q}\rho)}{k_{\rho q}\partial\rho}A_q(k_z)-(-i)^m\frac{mJ_m(k_{\rho q}\rho)}{k_{\rho q}\rho}B_q(k_z)\right]e^{-i(k_z z+m\phi)+i(m-n)\phi_k}\\&=2\pi(-i)^n\left[\frac{i\partial J_n(k_{\rho q}\rho)A_q(k_z)}{k_{\rho q}\partial\rho}-\frac{nJ_n(k_{\rho q}\rho)B_q(k_z)}{k_{\rho q}\rho}\right]e^{-i(k_z z+n\phi)}\end{aligned} \tag{A5}$$

$$\begin{aligned}Q_n(k_z)&=\int_{\phi_k=0}^{2\pi}d\phi_k\sum_{m=-\infty}^{\infty}\left[(-i)^{m-1}\frac{\partial J_m(k_{\rho q}\rho)}{k_{\rho q}\partial\rho}B_q(k_z)+(-i)^m\frac{mJ_m(k_{\rho q}\rho)}{k_{\rho q}\rho}A_q(k_z)\right]e^{-i(k_z z+m\phi)+i(m-n)\phi_k}\\&=2\pi(-i)^n\left[\frac{i\partial J_n(k_{\rho q}\rho)B_q(k_z)}{k_{\rho q}\partial\rho}+\frac{nJ_n(k_{\rho q}\rho)A_q(k_z)}{k_{\rho q}\rho}\right]e^{-i(k_z z+n\phi)},\end{aligned} \tag{A6}$$

and

$$\begin{aligned}R_n(k_z)&=\int_{\phi_k=0}^{2\pi}d\phi_k\sum_{m=-\infty}^{\infty}[(-i)^mJ_m(k_{\rho q}\rho)]\times e^{-i(k_z z+m\phi)+i(m-n)\phi_k}\\&=2\pi(-i)^nJ_n(k_{\rho q}\rho)e^{-i(k_z z+n\phi)}\end{aligned} \tag{A7}$$

By introducing the cylindrical vector wave functions (13a)–(13c) and recalling the complete property of this set of functions [3,25], it is reasonable to assume the electric field in a uniaxial chiral medium can be represented in the form of Eq. (12). Then, comparing the coordinate components of Eq. (12) with those of Eq. (A4) where $P_n(k_z)$, $Q_n(k_z)$, and $R_n(k_z)$ are determined by Eqs. (A5)–(A7), we derive a set of equations

$$A_q^e(k_z)=-\frac{2i}{k_{\rho q}}B_q(k_z), \tag{A8}$$

$$\frac{k_z}{k_q}B_q^e(k_z)+iC_q^e(k_z)=-\frac{2}{k_{\rho q}}A_q(k_z), \tag{A9}$$

and

$$\frac{k_{\rho q}^2}{k_q}B_q^e(k_z)-ik_zC_q^e(k_z)=2. \tag{A10}$$

The solutions to this set of linear equations (A8)–(A10), in conjunction with Eqs. (7a) and (7b), result in the expressions of Eqs. (14a)–(14c).

APPENDIX B: DETAILED PROCEDURE FOR THE SOLUTIONS OF EQS. (20a)–(20d)

For simplicity, we introduce

$$V_{qn}^{p(j)}(\rho)=-\frac{in}{\rho}Z_n^{(j)}(k_{\rho q}\rho)C_q^p(k_z=0)-k_{\rho q}Z_n^{(j)\prime}(k_{\rho q}\rho)\times A_q^p(k_z=0), \tag{B1}$$

$$X_{qn}^p(\rho)=K_{\rho q}J_n(k_{\rho q}\rho)B_q^p(k_z=0), \tag{B2}$$

$$Y_{qn}^{p(j)}(\rho)=-\frac{in}{\rho}Z_n^{(j)}(k_{\rho q}\rho)A_q^p(k_z=0)+k_{\rho q}Z_n^{(j)\prime}(k_{\rho q}\rho)\times C_q^p(k_z=0), \tag{B3}$$

where $\rho=f(\phi)$, $q=1$ and 2, and $p=e$ and h.

Multiplying both sides of Eqs. (20a)–(20d) with $e^{im\phi}(m=-N,-N+1,...,N-1,N)$ and integrating from 0 to 2π, we end up with

$$\sum_{q=1}^{2}[\mathbf{I}^{qe}][\mathbf{e}_q]=[\mathbf{I}^{(2)}][\mathbf{a}], \tag{B4}$$

$$\sum_{q=1}^{2}[\mathbf{I}^{qh}][\mathbf{e}_q]+\frac{k_0}{i\omega\mu_0}[\mathbf{I}^{(2)}][\mathbf{b}]=[\mathbf{P}][\mathbf{I}], \tag{B5}$$

$$\sum_{q=1}^{2}[\mathbf{A}^{qe}][\mathbf{e}_q]-[\mathbf{I}^{(5)}][\mathbf{b}]=[\mathbf{Q}][\mathbf{I}], \tag{B6}$$

$$\sum_{q=1}^{2}[\mathbf{A}^{qh}][\mathbf{e}_q]=-\frac{k_0}{i\omega\mu_0}[\mathbf{I}^{(5)}][\mathbf{a}], \tag{B7}$$

where $[\mathbf{a}]$ and $[\mathbf{b}]$ are column vectors of the expansion coefficients of the scattered waves, respectively, and

$$(I^{qp})_{mn}=\int_{\phi=0}^{2\pi}(-i)^{n'}e^{-i(n'-m')\phi}[Y_{qn'}^p(\rho)\sin\theta+V_{qn'}^p(\rho)\cos\theta]d\phi, \tag{B8}$$

$$(I^{(2)})_{mn}=\int_{\phi=0}^{2\pi}(-i)^{n'}e^{-i(n'-m')\phi}\left[-\frac{in'}{\rho}H_{n'}^{(2)}(k_0\rho)\sin\theta-k_0H_{n'}^{(2)\prime}(k_0\rho)\cos\theta\right]d\phi, \tag{B9}$$

$$(P)_{nm}=\frac{1}{i\omega\mu_0}\int_{\phi=0}^{2\pi}(-i)^{n'}e^{-i(n'-m')\phi}\left[\frac{in}{\rho}J_{n'}(k_0\rho)\sin\theta+k_0J_{n'}'(k_0\rho)\cos\theta\right]d\phi, \tag{B10}$$

$$(Q)_{nm}=\int_{\phi=0}^{2\pi}(-i)^{n'}e^{-i(n'-m')\phi}J_{n'}(k_0\rho)d\phi, \tag{B11}$$

$$(A^{qp})_{mn}=\int_{\phi=0}^{2\pi}(-i)^{n'}e^{-i(n'-m')\phi}X_{qn'}^{p}(\rho)d\phi, \tag{B12}$$

$$(I^{(5)})_{mn}=\int_{\phi=0}^{2\pi}(-i)^{n'}e^{-i(n'-m')\phi}k_0H_{n'}^{(2)}(k_0\rho)d\phi \tag{B13}$$

for $q=1$ or 2, $p=e$ or h, $m,\ n\in[1,2N+1]$, and $m'=m-(N+1)$, $n'=n-(N+1)$. Here $[\mathbf{I}]$ is the $(2N+1)$-dimension unit vector, and the primes over the Bessel and Hankel functions denote the derivatives with respect to the arguments.

Straightforward algebraic manipulation for Eqs. (B4)–(B7), we obtain

$$[\mathbf{a}]=\left[\frac{i\omega\mu_0}{k_0}[\mathbf{I}^{(2)}]^{-1}[\mathbf{D}^{(1)}]+[\mathbf{I}^{(5)}]^{-1}[\mathbf{D}^{(2)}]\right]^{-1}\left[\frac{i\omega\mu_0}{k_0}[\mathbf{I}^{(2)}]^{-1}[\mathbf{P}]+[\mathbf{I}^{(5)}]^{-1}[\mathbf{Q}]\right], \tag{B14}$$

$$[\mathbf{b}]=\left[\frac{k_0}{i\omega\mu_0}[\mathbf{D}^{(1)}]^{-1}[\mathbf{I}^{(2)}]+[\mathbf{D}^{(2)}]^{-1}[\mathbf{I}^{(5)}]\right]^{-1}[[\mathbf{D}^{(1)}]^{-1}[\mathbf{P}]-[\mathbf{D}^{(2)}]^{-1}[\mathbf{Q}]], \tag{B15}$$

where

$$[\mathbf{D}^{(1)}]=[\mathbf{I}^{1h}][\mathbf{C}^{(2)}]+[\mathbf{I}^{2h}][\mathbf{C}^{(1)}], \tag{B16}$$

$$[\mathbf{D}^{(2)}]=[\mathbf{A}^{1e}][\mathbf{C}^{(2)}]+[\mathbf{A}^{2h}][\mathbf{C}^{(1)}], \tag{B17}$$

and

$$[\mathbf{C}^{(1)}]=[[\mathbf{I}^{1e}]^{-1}[\mathbf{I}^{2e}]-[\mathbf{A}^{1h}]^{-1}[\mathbf{A}^{2h}]]^{-1}\left[[\mathbf{I}^{1e}]^{-1}[\mathbf{I}^{(2)}]+\frac{k_0}{i\omega\mu_0}[\mathbf{A}^{1h}]^{-1}[\mathbf{I}^{(5)}]\right], \tag{B18}$$

$$[\mathbf{C}^{(2)}]=[[\mathbf{I}^{2e}]^{-1}[\mathbf{I}^{1e}]-[\mathbf{A}^{2h}]^{-1}[\mathbf{A}^{1h}]]^{-1}\left[[\mathbf{I}^{2e}]^{-1}[\mathbf{I}^{(2)}]+\frac{k_0}{i\omega\mu_0}[\mathbf{A}^{2h}]^{-1}[\mathbf{I}^{(5)}]\right]. \tag{B19}$$

After numerically evaluating the matrices involved, Eqs. (B14) and (B15) would result in the expansion coefficients of the scattered fields.

APPENDIX C: ELECTROMAGNETIC SCATTERING BY A UNIAXIAL CHIRAL CIRCULAR CYLINDER

Here, we will present explicit expressions of expansion coefficients of the scattered field for the scattering of a uniaxial chiral circular cylinder of radius ρ_0. In the case of a TM_z-polarized incident plane wave illuminating along the $+x$ axis, incident electromagnetic fields can be expanded in terms of the circular cylindrical vector wave functions, as presented in Eqs. (18a) and (18b). The electromagnetic fields excited inside the scatterer can be represented in terms of the cylindrical vector wave functions in the way we presented in Sec. II. Also, the scattered electromagnetic waves may have TM_z and TE_z components, and should be expanded as Eqs. (19a) and (19b).

Applying the widely employed mode-matching method [12,25] to have the boundary conditions of continuous tangential electric and magnetic fields satisfied at the outer surface of the scatterer $\rho=\rho_0$, the expansion coefficients of the scattered fields are derived as

$$a_n=-\frac{2E_0}{\pi\eta_0\rho_0\Delta_n(\rho_0)}\,\delta(k_z)[V_{1n}^{e}(\rho_0)X_{2n}^{h}(\rho_0)-V_{2n}^{e}(\rho_0)X_{1n}^{h}(\rho_0)] \tag{C1}$$

and

$$b_n=\frac{E_0}{\Delta_n(\rho_0)}\,\delta(k_z)\left[J_n(k_0\rho_0)C_n(\rho_0)+\frac{i}{\eta_0}J_n'(k_0\rho_0)D_n(\rho_0)\right], \tag{C2}$$

where

$$V_{qn}^{p}(\rho_0)=A_q^p(k_z)k_{\rho q}J_n'(k_{\rho q}\rho_0)+\frac{in}{\rho_0}C_q^p(k_z)J_n(k_{\rho q}\rho_0), \tag{C3}$$

$$X_{qn}^{p}(\rho_0)=B_q^p(k_z)k_{\rho q}J_n(k_{\rho q}\rho_0) \tag{C4}$$

for $q=1$ and 2 and $p=e$ and h. In Eqs. (C1) and (C2),

$$C_n(\rho_0)=-k_0H_n^{(2)'}(k_0\rho_0)[V_{1n}^{h}(\rho_0)X_{2n}^{h}(\rho_0)-V_{2n}^{h}(\rho_0)X_{1n}^{h}(\rho_0)]-i\omega\varepsilon_0H_n^{(2)}[V_{1n}^{e}(\rho_0)V_{2n}^{h}(\rho_0)-V_{2n}^{e}(\rho_0)V_{1n}^{h}(\rho_0)], \tag{C5}$$

$$D_n(\rho_0)=k_0H_n^{(2)'}(k_0\rho_0)[X_{1n}^{e}(\rho_0)X_{2n}^{h}(\rho_0)-X_{2n}^{e}(\rho_0)X_{1n}^{h}(\rho_0)]+i\omega\varepsilon_0H_n^{(2)}[V_{1n}^{e}(\rho_0)X_{2n}^{e}(\rho_0)-V_{2n}^{e}(\rho_0)X_{1n}^{e}(\rho_0)], \tag{C6}$$

$$\Delta_n(\rho_0)=-k_0H_n^{(2)}(k_0\rho_0)C_n(\rho_0)-i\omega\varepsilon_0H_n^{(2)'}(k_0\rho_0)D_n(\rho_0). \tag{C7}$$

Due to the emergence of the Dirac delta function $\delta(k_z)$ in Eq. (C1) and (C2), the infinite integration of the k_z variable for the scattered fields has actually disappeared. Using the asymptotic expression of the Hankel function in the far region, Eq. (22), the bistatic echo width of this structure Eq. (21) can be rewritten in a more explicit form

$$A_\sigma(\phi)=\frac{4}{k_0E_0^2}\left[\left|\sum_{n=0}^{\infty}(-1)^n\delta_n a_n\cos(n\phi)\right|^2+\left|\sum_{n=0}^{\infty}(-1)^n\delta_n b_n\cos(n\phi)\right|^2\right], \tag{C8}$$

where δ_n is the Neumann factor, i.e., $\delta_n=1$ for $n=0$, and 2 for $n>0$.

APPENDIX D: SOLUTIONS FOR SCATTERING COEFFICIENTS OF A CONDUCTING CIRCULAR CYLINDER WITH AN INHOMOGENEOUS COATING THICKNESS OF UNIAXIAL CHIRAL MEDIUM

For simplicity, we introduce

$$V_{qn}^{p(j)}(\rho)=-\frac{in}{\rho}Z_n^{(j)}(k_{\rho q}\rho)C_q^p(k_z=0)-k_{\rho q}Z_n^{(j)'}(k_{\rho q}\rho)\times A_q^p(k_z=0), \tag{D1}$$

$$X_{qn}^{p(j)}(\rho)=k_{\rho q}Z_n^{(j)}(k_{\rho q}\rho)B_q^p(k_z=0), \tag{D2}$$

$$Y_{qn}^{p(j)}(\rho)=-\frac{in}{\rho}Z_n^{(j)}(k_{\rho q}\rho)A_q^p(k_z=0)+k_{\rho q}Z_n^{(j)'}(k_{\rho q}\rho)\times C_q^p(k_z=0), \tag{D3}$$

where $\rho=f(\phi)$ or $\rho=a$, $q=1$ or 2, $p=e$ or h, and $Z_n^{(j)}(\,)=J_n(\,)$ or $Z_n^{(j)}(\,)=H_n^{(2)}(\,)$ for $j=1$ and 4, respectively.

From the boundary conditions Eqs. (25a) and (25b) at $\rho=a$, we have

$$[\mathbf{e}_1^{(4)}]=[\mathbf{A}^{11}][\mathbf{e}_1^{(1)}]+[\mathbf{A}^{12}][\mathbf{e}_2^{(1)}], \tag{D4}$$

$$[\mathbf{e}_2^{(4)}]=[\mathbf{A}^{21}][\mathbf{e}_1^{(1)}]+[\mathbf{A}^{22}][\mathbf{e}_2^{(1)}] \tag{D5}$$

where $[\mathbf{e}_q^{(j)}]$ (for $q=1$ or 2 and $j=1$ or 4) are column vectors of the expansion coefficients for the internal fields of the coating, and

$$[\mathbf{A}^{11}]=[[\mathbf{X}^{2(4)}]^{-1}[\mathbf{X}^{1(4)}]-[\mathbf{V}^{2(4)}]^{-1}[\mathbf{V}^{1(4)}]]^{-1}[[\mathbf{V}^{2(4)}]^{-1}[\mathbf{V}^{1(1)}]-[\mathbf{X}^{2(4)}]^{-1}[\mathbf{X}^{1(1)}]], \tag{D6}$$

$$[\mathbf{A}^{12}]=[[\mathbf{X}^{2(4)}]^{-1}[\mathbf{X}^{1(4)}]-[\mathbf{V}^{2(4)}]^{-1}[\mathbf{V}^{1(4)}]]^{-1}[[\mathbf{V}^{2(4)}]^{-1}[\mathbf{V}^{2(1)}]-[\mathbf{X}^{2(4)}]^{-1}[\mathbf{X}^{2(1)}]], \tag{D7}$$

$$[\mathbf{A}^{21}]=[[\mathbf{X}^{1(4)}]^{-1}[\mathbf{X}^{2(4)}]-[\mathbf{V}^{1(4)}]^{-1}[\mathbf{V}^{2(4)}]]^{-1}[[\mathbf{V}^{1(4)}]^{-1}[\mathbf{V}^{1(1)}]-[\mathbf{X}^{1(4)}]^{-1}[\mathbf{X}^{1(1)}]], \tag{D8}$$

$$[\mathbf{A}^{22}]=[[\mathbf{X}^{1(4)}]^{-1}[\mathbf{X}^{2(4)}]-[\mathbf{V}^{1(4)}]^{-1}[\mathbf{V}^{2(4)}]]^{-1}[[\mathbf{V}^{1(4)}]^{-1}[\mathbf{V}^{2(1)}]-[\mathbf{X}^{1(4)}]^{-1}[\mathbf{X}^{2(1)}]], \tag{D9}$$

and the matrices involved in Eqs. (D6)–(D9) are all diagonal with the diagonal elements given as

$$(X_p^{q(j)})_{mn}=X_{qn'}^{p(j)}(\rho=a)\,\delta(m'-n'), \tag{D10}$$

$$(V_p^{q(j)})_{mn}=V_{qn'}^{p(j)}(\rho=a)\,\delta(m'-n') \tag{D11}$$

for $m,n\in[1,2N+1]$ and $m'=m-(N+1)$, $n'=n-(N+1)$.

After substituting Eqs. (D4) and (D5) into Eqs. (26a)–(26d), multiplying both sides of the resulting equations with $e^{im\phi}$ $(m=-N,-N+1,...,N-1,N)$, and integrating from 0 to 2π, we end up with

$$\sum_{q=1}^{2}[\mathbf{I}^{qe}][\mathbf{e}_q^{(1)}]=[\mathbf{I}^{(2)}][\mathbf{a}], \tag{D12}$$

$$\sum_{q=1}^{2}[\mathbf{I}^{qh}][\mathbf{e}_q^{(1)}]+\frac{k_0}{i\omega\mu_0}[\mathbf{I}^{(2)}][\mathbf{b}]=[\mathbf{P}][\mathbf{I}], \tag{D13}$$

$$\sum_{q=1}^{2}[\mathbf{A}^{qe}][\mathbf{e}_q^{(1)}]-[\mathbf{I}^{(5)}][\mathbf{b}]=[\mathbf{Q}][\mathbf{I}], \tag{D14}$$

$$\sum_{q=1}^{2}[\mathbf{A}^{qh}][\mathbf{e}_q^{(1)}]=-\frac{k_0}{i\omega\mu_0}[\mathbf{I}^{(5)}][\mathbf{a}], \tag{D15}$$

where $[\mathbf{a}]$ and $[\mathbf{b}]$ are column vectors of the expansion coefficients of the scattered waves, and

$$[\mathbf{I}^{qp}]=[\mathbf{B}_p^{q(1)}]+[\mathbf{B}_p^{1(4)}][\mathbf{A}^{1q}]+[\mathbf{B}_p^{2(4)}][\mathbf{A}^{2q}], \tag{D16}$$

$$[\mathbf{A}^{qp}]=[\mathbf{C}_p^{q(1)}]+[\mathbf{C}_p^{1(4)}][\mathbf{A}^{1q}]+[\mathbf{C}_p^{2(4)}][\mathbf{A}^{2q}], \tag{D17}$$

with

$$(B_p^{q(j)})_{mn}=\int_{\phi=0}^{2\pi}(-i)^{n'}e^{-i(n'-m')\phi}[Y_{qn'}^{p(j)}(\rho)\sin\theta+V_{qn'}^{p(j)}(\rho)\cos\theta]d\phi, \tag{D18}$$

$$(I^{(2)})_{mn}=\int_{\phi=0}^{2\pi}(-i)^{n'}e^{-i(n'-m')\phi}\left[-\frac{in'}{\rho}H_{n'}^{(1)}(k_0\rho)\sin\theta-k_0H_{n'}^{(1)'}(k_0\rho)\cos\theta\right]d\phi, \tag{D19}$$

$$(P)_{nm}=\frac{1}{i\omega\mu_0}\int_{\phi=0}^{2\pi}(-i)^{n'}e^{-i(n'-m')\phi}\left[\frac{in'}{\rho}J_{n'}(k_0\rho)\sin\theta+k_0J_{n'}'(k_0\rho)\cos\theta\right]d\phi, \tag{D20}$$

$$(Q)_{nm}=\int_{\phi=0}^{2\pi}(-i)^{n'}e^{-i(n'-m')\phi}J_{n'}(k_0\rho)d\phi, \tag{D21}$$

$$(C_p^{q(j)})_{mn}=\int_{\phi=0}^{2\pi}(-i)^{n'}e^{-i(n'-m')\phi}X_{qn'}^{p(j)}(\rho)d\phi, \tag{D22}$$

$$(I^{(5)})_{mn}=\int_{\phi=0}^{2\pi}(-i)^{n'}e^{-i(n'-m')\phi}k_0H_{n'}^{(2)}(k_0\rho)d\phi \tag{D23}$$

for $q=1$ or 2, and $p=e$ or h.

Straightforward algebraic manipulation for Eqs. (D12)–(D15) yields

$$[\mathbf{a}]=\left[\frac{i\omega\mu_0}{k_0}[\mathbf{I}^{(2)}]^{-1}[\mathbf{D}^{(1)}]+[\mathbf{I}^{(5)}]^{-1}[\mathbf{D}^{(2)}]\right]^{-1}\left[\frac{i\omega\mu_0}{k_0}[\mathbf{I}^{(2)}]^{-1}[\mathbf{P}]+[\mathbf{I}^{(5)}]^{-1}[\mathbf{Q}]\right], \tag{D24}$$

$$[\mathbf{b}]=\left[\frac{k_0}{i\omega\mu_0}[\mathbf{D}^{(1)}]^{-1}[\mathbf{I}^{(2)}]+[\mathbf{D}^{(2)}]^{-1}[\mathbf{I}^{(5)}]\right]^{-1}[[\mathbf{D}^{(1)}]^{-1}[\mathbf{P}]-[\mathbf{D}^{(2)}]^{-1}[\mathbf{Q}]], \tag{D25}$$

where

$$[\mathbf{D}^{(1)}]=[\mathbf{I}^{1h}][\mathbf{C}^{(2)}]+[\mathbf{I}^{2h}][\mathbf{C}^{(1)}], \tag{D26}$$

$$[\mathbf{D}^{(2)}]=[\mathbf{A}^{1e}][\mathbf{C}^{(2)}]+[\mathbf{A}^{2h}][\mathbf{C}^{(1)}], \tag{D27}$$

and

$$[\mathbf{C}^{(1)}]=[[\mathbf{I}^{1e}]^{-1}[\mathbf{I}^{2e}]-[\mathbf{A}^{1h}]^{-1}[\mathbf{A}^{2h}]]^{-1}\left[[\mathbf{I}^{1e}]^{-1}[\mathbf{I}^{(2)}]+\frac{k_0}{i\omega\mu_0}[\mathbf{A}^{1h}]^{-1}[\mathbf{I}^{(5)}]\right], \tag{D28}$$

$$[\mathbf{C}^{(2)}]=[[\mathbf{I}^{2e}]^{-1}[\mathbf{I}^{1e}]-[\mathbf{A}^{2h}]^{-1}[\mathbf{A}^{1h}]]^{-1}\left[[\mathbf{I}^{2e}]^{-1}[\mathbf{I}^{(2)}]+\frac{k_0}{i\omega\mu_0}[\mathbf{A}^{2h}]^{-1}[\mathbf{I}^{(5)}]\right]. \tag{D29}$$

APPENDIX E: DETAILS OF THE SCATTERING OF TWO UNIAXIAL CHIRAL CIRCULAR CYLINDERS

The boundary conditions at $\rho_1=a_1$ can be written as

$$[\mathbf{A}_1^{(1)}][\mathbf{a}^{\text{inc}}]+[\mathbf{B}_1^{(1)}][\mathbf{a}^{(1)}]+[\mathbf{C}_1^{(1)}][\mathbf{a}^{(2)}]=\sum_{q=1}^{2}[\mathbf{D}_q^{e(1)}][\mathbf{e}_q^{(1)}], \tag{E1}$$

$$[\mathbf{A}_1^{(1)}][\mathbf{b}^{\text{inc}}]+[\mathbf{B}_1^{(1)}][\mathbf{b}^{(1)}]+[\mathbf{C}_1^{(1)}][\mathbf{b}^{(2)}]=-\frac{i\omega\mu_0}{k_0}\sum_{q=1}^{2}[\mathbf{D}_q^{h(1)}][\mathbf{e}_q^{(1)}], \tag{E2}$$

$$[\mathbf{A}_2^{(1)}][\mathbf{a}^{\text{inc}}]+[\mathbf{B}_2^{(1)}][\mathbf{a}^{(1)}]+[\mathbf{C}_2^{(1)}][\mathbf{a}^{(2)}]=-\frac{i\omega\mu_0}{k_0}\sum_{q=1}^{2}[\mathbf{E}_q^{h(1)}][\mathbf{e}_q^{(1)}], \tag{E3}$$

$$[\mathbf{A}_2^{(1)}][\mathbf{b}^{\text{inc}}]+[\mathbf{B}_2^{(1)}][\mathbf{b}^{(1)}]+[\mathbf{C}_2^{(1)}][\mathbf{b}^{(2)}]=\sum_{q=1}^{2}[\mathbf{E}_q^{e(1)}][\mathbf{e}_q^{(1)}], \tag{E4}$$

and the boundary conditions at $\rho_2=a_2$ can be written as

$$[\mathbf{A}_1^{(2)}][\mathbf{a}^{\text{inc}}]+[\mathbf{C}_1^{(2)}][\mathbf{a}^{(1)}]+[\mathbf{B}_1^{(2)}][\mathbf{a}^{(2)}]=\sum_{q=1}^{2}[\mathbf{D}_q^{e(2)}][\mathbf{e}_q^{(2)}], \tag{E5}$$

$$[\mathbf{A}_1^{(2)}][\mathbf{b}^{\text{inc}}]=[\mathbf{C}_1^{(2)}][\mathbf{b}^{(1)}]+[\mathbf{B}_1^{(2)}][\mathbf{b}^{(2)}]=-\frac{i\omega\mu_0}{k_0}\sum_{q=1}^{2}[\mathbf{D}_q^{h(2)}][\mathbf{e}_q^{(2)}], \tag{E6}$$

$$[\mathbf{A}_2^{(2)}][\mathbf{a}^{\text{inc}}]+[\mathbf{C}_2^{(2)}][\mathbf{a}^{(1)}]+[\mathbf{B}_2^{(2)}][\mathbf{a}^{(2)}]=-\frac{i\omega\mu_0}{k_0}\sum_{q=1}^{2}[\mathbf{E}_q^{h(2)}][\mathbf{e}_q^{(2)}], \tag{E7}$$

$$[\mathbf{A}_2^{(2)}][\mathbf{b}^{\text{inc}}]+[\mathbf{C}_2^{(2)}][\mathbf{b}^{(1)}]+[\mathbf{B}_2^{(2)}][\mathbf{b}^{(2)}]=\sum_{q=1}^{2}[\mathbf{E}_q^{e(2)}][\mathbf{e}_q^{(2)}], \tag{E8}$$

where

$$(A_1^{(j)})_{mn}=(-i)^{n'}J_{m'-n'}(k_0d)e^{i(m'-n')\phi_j}J'_{m'}(k_0a_j), \tag{E9}$$

$$(A_2^{(j)})_{mn}=(-i)^{n'}J_{m'-n'}(k_0d)e^{i(m'-n')\phi_j}J_{m'}(k_0a_j), \tag{E10}$$

$$(B_1^{(j)})_{mn}=(-i)^{n'}H_{n'}^{(2)'}(k_0a_j)\,\delta(m'-n'), \tag{E11}$$

$$(B_2^{(j)})_{mn}=(-i)^{n'}H_{n'}^{(2)}(k_0a_j)\,\delta(m'-n'), \tag{E12}$$

$$(C_1^{(j)})_{mn}=(-i)^{n'}H_{m'-n'}^{(2)}(2k_0d)e^{i(m'-n')\phi_j}J_{m'}(k_0a_j), \tag{E13}$$

$$(C_2^{(j)})_{mn}=(-i)^{n'}H_{m'-n'}^{(2)}(2k_0d)e^{i(m'-n')\phi_j}J_{m'}'(k_0a_j), \tag{E14}$$

$$(D_q^{p(j)})_{mn}=\frac{(-i)^{n'}}{k_0}\left[k_{\rho q}^{(j)}J_{n'}'(k_{\rho q}^{(j)}a_j)A_q^{p(j)}(k_z=0)+\frac{in'}{\rho_j}J_{n'}(k_{\rho q}^{(j)}a_j)C_q^{p(j)}(k_z=0)\right]\delta(m'-n'), \tag{E15}$$

$$(E_q^{p(j)})_{mn}=\frac{(-i)^{n'}}{k_0}k_{\rho q}^{(j)}(k_{\rho q}^{(j)}a_j)B_q^{p(j)}(k_z=0)\,\delta(m'-n'), \tag{E16}$$

with $\phi_1=0$, $\phi_2=\pi$, $j=1$ or 2, $p=e$ or h, $m,n\in[1,2N+1]$, and $m'=m-(N+1)$, $n'=n-(N+1)$. Straightforward manipulation of Eqs. (E1)–(E8) will give rise to solutions of the scattering coefficient vectors $[\mathbf{a}^{(1)}]$, $[\mathbf{b}^{(1)}]$, and $[\mathbf{a}^{(2)}]$, $[\mathbf{b}^{(2)}]$, respectively.

[1] W. W. Hansen, Phys. Rev. **47**, 139 (1935).
[2] J. A. Stratton, *Electromagnetic Theory* (McGraw-Hill, New York, 1941).
[3] P. Morse and H. Feshbach, *Methods of Theoretical Physics* (McGraw-Hill, New York, 1953).
[4] C. T. Tai, *Dyadic Green's Functions in Electromagnetic Theory* (Intertext, New York, 1971).
[5] R. D. Graglia, P. L. E. Uslenghi, and R. S. Zich, Proc. IEEE **77**, 750 (1989).
[6] V. V. Varadan, A. Lakhtakia, and V. K. Varadan, IEEE Trans. Antennas Propag. **37**, 800 (1989).
[7] S. N. Papadakis, N. K. Uzunoglu, and N. Christos, J. Opt. Soc. Am. A **7**, 991 (1990).
[8] D. Cheng, Phys. Rev. E **50**, 4107 (1994).
[9] D. Cheng and W. Ren, Phys. Rev. E **54**, 2917 (1996).
[10] D. Cheng, Phys. Rev. E **56**, 2321 (1997).
[11] D. Cheng, Phys. Rev. E **55**, 1950 (1997).
[12] J. A. Kong, *Theory of Electromagnetic Waves* (Wiley, New York, 1975).
[13] C. Yeh, J. Math. Phys. **6**, 2008 (1965).
[14] *Acoustic Electromagnetic and Elastic Wave Scattering-Focus on the T-Matrix Approach*, edited by V. K. Varadan and V. V. Varadan (Pergamon, New York, 1980).
[15] E. J. Rothwell and L. L. Frasch, IEEE Trans. Microwave Theory Tech. **36**, 594 (1988).
[16] C. Hafner, *The Generalized Multipole Technique for Computational Electromagnetics* (Artech, London, 1990).
[17] I. V. Lindell, A. H. Sihvola, S. A. Tretyakov, and A. J. Viitanen, *Electromagnetic Waves in Chiral and Bianisotropic Media* (Artech, Norwood, 1994).
[18] *Bianisotropic and Biisotropic Media and Applications*, edited by A. Priou (EMW, Boston, 1994).
[19] N. Engheta, J. Electromagn. Waves Appl. **6**, 537 (1992).
[20] A. J. Viitanen and I. V. Lindell, Electron. Lett. **29**, 1074 (1993).
[21] A. J. Viitanen and I. V. Lindell, Int. J. Infrared Millim. Waves **14**, 1993 (1993).
[22] I. V. Lindell and A. H. Sihvola, IEEE Trans. Antennas Propag. **43**, 1397 (1995).
[23] E. J. Post, *Formal Structures of Electromagnetic* (North-Holland, Amsterdam, 1962).
[24] H. C. Chen, *Theory of Electromagnetic Waves—A Coordinate Free Approach* (McGraw-Hill, New York, 1983).
[25] W. C. Chew, *Waves and Fields in Inhomogeneous Media* (Van Nostrand, New York, 1990).
[26] R. J. Pogorzelski and E. Lun, Radio Sci. **11**, 753 (1976).